nature structural & molecular biology

Structural mechanism of allosteric substrate specificity regulation in a ribonucleotide reductase

Karl-Magnus Larsson[1], Albert Jordan[2,4], Rolf Eliasson[2], Peter Reichard[2], Derek T Logan[3] & Pär Nordlund[1]

Ribonucleotide reductases (RNRs) catalyze the reduction of ribonucleotides into deoxyribonucleotides, which constitute the precursor pools used for DNA synthesis and repair. Imbalances in these pools increase mutational rates and are detrimental to the cell. Balanced precursor pools are maintained primarily through the regulation of the RNR substrate specificity. Here, the molecular mechanism of the allosteric substrate specificity regulation is revealed through the structures of a dimeric coenzyme B12–dependent RNR from *Thermotoga maritima*, both in complexes with four effector-substrate nucleotide pairs and in three complexes with only effector. The mechanism is based on the flexibility of loop 2, a key structural element, which forms a bridge between the specificity effector and substrate nucleotides. Substrate specificity is achieved as different effectors and their cognate substrates stabilize specific discrete loop 2 conformations. The mechanism of substrate specificity regulation is probably general for most class I and class II RNRs.

RNRs are found in all living cells and provide the deoxyribonucleotides needed for DNA synthesis and repair (reviewed in ref. 1). In the reduction of the 2′ OH group of ribonucleotides, all RNRs use a sophisticated radical-based chemistry, and they have been divided into three classes[1] on the basis of their primary radical: the aerobic class I RNRs consist of two homodimers of two proteins (R1 and R2) and harbor a stable tyrosyl radical; the dimeric anaerobic class III RNRs contain a stable glycyl radical[2]; class II RNRs exist among both aerobic and anaerobic bacteria and generate a transient 5′-deoxyadenosyl radical through homolytic cleavage of the C-Co bond in adenosylcobalamin (coenzyme B12). In spite of this diversity, RNRs have a common active site cysteine to which the primary radical is transferred. A proposed cysteinyl radical thereafter abstracts the 3′ H from the substrate ribose, activating the substrate for reduction of the 2′ C-O bond[3,4].

RNRs catalyze the reduction of all four ribonucleotides while maintaining balanced pools of the product deoxyribonucleotides through a unique and complex feedback allosteric regulation[1,5]. This regulation is critical as an imbalance in the DNA precursor (dNTP) pools can cause disease owing to errors in DNA synthesis and repair[6]. The general pattern for this regulation was already established in the 1960s[7], although the molecular mechanism has been elusive. The system is based on two types of regulatory sites: activity and specificity sites. ATP or dATP bind to the activity site[5], where ATP stimulates overall activity and dATP turns the enzyme off. Class Ib RNRs, all presently characterized class II enzymes[8] and the class III RNR from bacteriophage T4 (refs. 9,10) lack this regulation. Substrate specificity is regulated via the specificity site, where ATP, dATP, dTTP, dGTP and (in a few cases) dCTP bind. The overall pattern of specificity regulation is common for all classes of RNR: ATP and dATP stimulate reduction of cytosine and uridine ribonucleotides, dTTP and dCTP stimulate reduction of guanosine ribonucleotides and dGTP stimulates reduction of adenosine ribonucleotides. The stimulation by effectors of the reduction of their corresponding cognate substrates is typically 10–100-fold.

The allosteric regulation of three class II RNRs has been studied[8,11–14]. The monomeric RNR from *Lactobacillus leichmannii* and the dimeric or higher oligomeric RNRs from *Thermoplasma acidophilum* and *Thermotoga maritima* have all been found to obey the general pattern of allosteric regulation, with the exception that dCTP is a potent effector for GDP reduction in the *T. acidophilum* enzyme. The overall activity is unaffected by dATP and ATP even though *T. acidophilum* contains an appropriate binding site.

Previous structural studies of RNRs have provided important but so far incomplete information on the structural basis for specificity regulation. The structure of the R1 protein of class I RNR from *Escherichia coli* in complex with its allosteric specificity effector dTTP and a partially defined substrate GDP[15] localized the specificity site to the dimer interface. Partial ordering of three loops (loops 1–3) in the vicinity of the effector was observed and these loops were proposed to be involved in allosteric signaling. Recently, structures of the related class Ib RNR from *Salmonella typhimurium*, in the apo form and in complex with dATP, dTTP and dCTP, reconfirmed the effector position, showed further movements in loops and revealed details of effector recognition[16]. The crystal structure of a class III RNR from bacteriophage T4 revealed a related α/β-barrel structure but with a

[1]Department of Biochemistry and Biophysics, Stockholm University, S-106 91 Stockholm, Sweden. [2]Department of Biochemistry, Karolinska Institute, S-171 77 Stockholm, Sweden. [3]Department of Molecular Biophysics, Lund University, Box 124, S-221 00 Lund, Sweden. [4]Current address: Centre for Genomic Regulation, Passeig Maritim 37–49, 08003 Barcelona, Spain. Correspondence should be addressed to P.N. (par@dbb.su.se) or D.T.L. (derek.logan@mbfys.lu.se).

Published online 10 October 2004; doi:10.1038/nsmb838

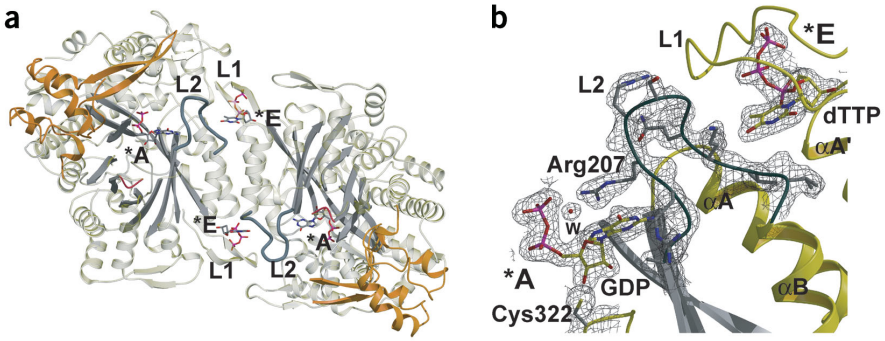

Figure 1 The structure of the *T. maritima* (tmNrdJ) dimeric ribonucleotide reductase. (**a**) Overall structure of tmNrdJ in complex with effector dTTP and substrate GDP. Loop 2 (L2) and the B12-binding domain (residues 500–575) are orange. Loop 2 bridges the specificity effector site (*E) and active sites (*A). (**b**) The allosteric specificity site, active site, loop 1 (L1) and loop 2 (L2) in the tmNrdJ–dTTP–GDP structure with the $2|F_o| - |F_c|$ map (contoured at 1 σ).

dimer interface and an effector-binding site highly divergent from those of class I RNRs[17]. The subsequent analysis of four structures of this RNR in complex with the substrate specificity effectors dATP, dTTP, dGTP and dCTP showed conformational changes upon binding of the different effectors, centered on loop 2 and ranging from subtle side chain movements to large-scale loop rearrangements[10].

The recent crystal structure of the monomeric class II RNR from *L. leichmannii* (llNrdJ)[18] revealed that a dimeric substrate specificity site is conserved in the monomeric enzyme through insertion of a 130-residue domain in the α/β-barrel, mimicking the monomer-monomer interactions involved in allosteric regulation, but no substrate or effector was bound. However the majority of currently characterized class II RNRs are dimeric and have effector sites highly homologous to those found in class I[8].

We present the first crystal structures of a dimeric class II RNR, from the hyperthermophile *T. maritima* (referred to as tmNrdJ[14]), in complex with four cognate allosteric specificity effector-substrate pairs, as well as structures with only the different effectors. These structures reveal for the first time the detailed molecular mechanism of substrate specificity regulation in a ribonucleotide reductase. The mechanism is likely to be general in most aspects for both class I and II RNRs, and has elements in common with the partial mechanism proposed for class III.

RESULTS

Overall structure of tmNrdJ

The structures are of an engineered fragment of tmNrdJ comprising residues 1–644 (lacking 645–827), which is similar to less well-defined, C-terminally truncated forms of tmNrdJ previously recovered after overproduction of the intact enzyme in *E. coli*[9]. The fragment lacks the C-terminal cysteines that transfer reducing equivalents to the active site from the natural redox partner thioredoxin, but is fully active in the presence of reduced DTT. In all other respects, including the allosteric substrate specificity regulation, the truncated form is indistinguishable from the complete enzyme (data not shown). The structure of tmNrdJ in the dTTP–GDP complex has been refined at 1.9 Å. The other structures are very similar except in the active site and specificity site. All data processing and refinement statistics are presented in **Table 1**. No apo form with an empty specificity site has been obtained as the 'native' tmNrdJ structure showed bound dATP, probably from a dATP-Sepharose purification step[8,14].

The overall structure of a tmNrdJ dimer (**Fig. 1**) is highly similar to the class I and II RNR structures[16,18,19], containing the canonical ten-stranded α/β-barrel of RNRs and pyruvate formate lyase[20,21].

Substrate binding

The residues implicated in the catalytic mechanism of class I and II RNRs are conserved (Cys134, Cys322, Cys333, Asn320 and Glu324) and positioned similarly (**Fig. 2a**) at the center of the ten-stranded α/β-barrel as in previously determined class I and II RNR structures[15,16,18]. The disulfide-forming cysteines Cys134 and Cys333 are in the reduced state. In the only previously determined substrate complex, *E. coli* R1–GDP, the substrate density was ambiguous, indicating partial occupancy or disordered binding[15]. In contrast, in the four different substrate nucleotide complexes of tmNrdJ, the density is unambiguous and supportive of full occupancy, although in the dATP–CDP structure only one of the active sites is fully occupied. The substrate phosphate groups are anchored at the ends of two helices that are structurally homologous to α12 and α24 in R1. The electron density unambiguously establishes the ribose ring pucker as C3′-*endo* in all substrates; in the *E. coli* R1 GDP structure, the ribose was modeled as nonpuckered. In all the tmNrdJ substrate complexes, Glu324 (Glu441 in R1) makes a double hydrogen bond to 3′ OH rather than the single hydrogen bond suggested from the R1 structure. Asn320 makes bridging hydrogen bonds to both 3′ OH and 2′ OH. An additional hydrogen bond to the main chain carbonyl of Ala133, which is adjacent to Cys134, one of the redox-active cysteines[4], further anchors the substrate. The Sγ atom of Cys322, expected to abstract the 3′ H atom from the substrate ribose[3], is at 3.5–4.1 Å from the ribose C3′ atom in the different complexes (**Fig. 2**). In general, the binding of the ribose is consistent with the previously proposed mechanism for ribonucleotide reduction[3,4], although the new ribose conformation and interactions might have implications for theoretical evaluations of the reaction mechanism[22].

Specific interactions of the substrate bases

The substrate bases are well defined in all the substrate–effector complexes. In the dTTP–GDP complex (**Fig. 2a,b**) the guanosine base fits into a tight pocket built by loop 2, the short turn (turn B) between αA and βB (159–160, called loop B in llNrdJ[18]), and Gly161 at the beginning of βB, which are all in the same monomer. All residues of loop 2 are well ordered and form a curved β-hairpin. The side chain methyl group of Ala210 makes a hydrophobic interaction with the base. A key side chain is that of Arg207 on loop 2, which stretches over of the base and ribose and makes a direct interaction with the substrate β-phosphate, thereby clamping the substrate into the active site, as the arginine guanidinyl moiety also makes π-π stacking interactions to the base. A well-ordered water molecule bridges the ribose, phosphates and Arg207. The direct specificity interactions in the dTTP–GDP complex consist of a hydrogen bond network from the substrate base to the substrate proximal edge of loop 2 and turn B (**Fig. 2a**), involving only main chain atoms. The positioning of several conserved small residues in this region seems both to make space for the large guanosine base and to achieve the necessary conformational flexibility for transition between different cognate complexes.

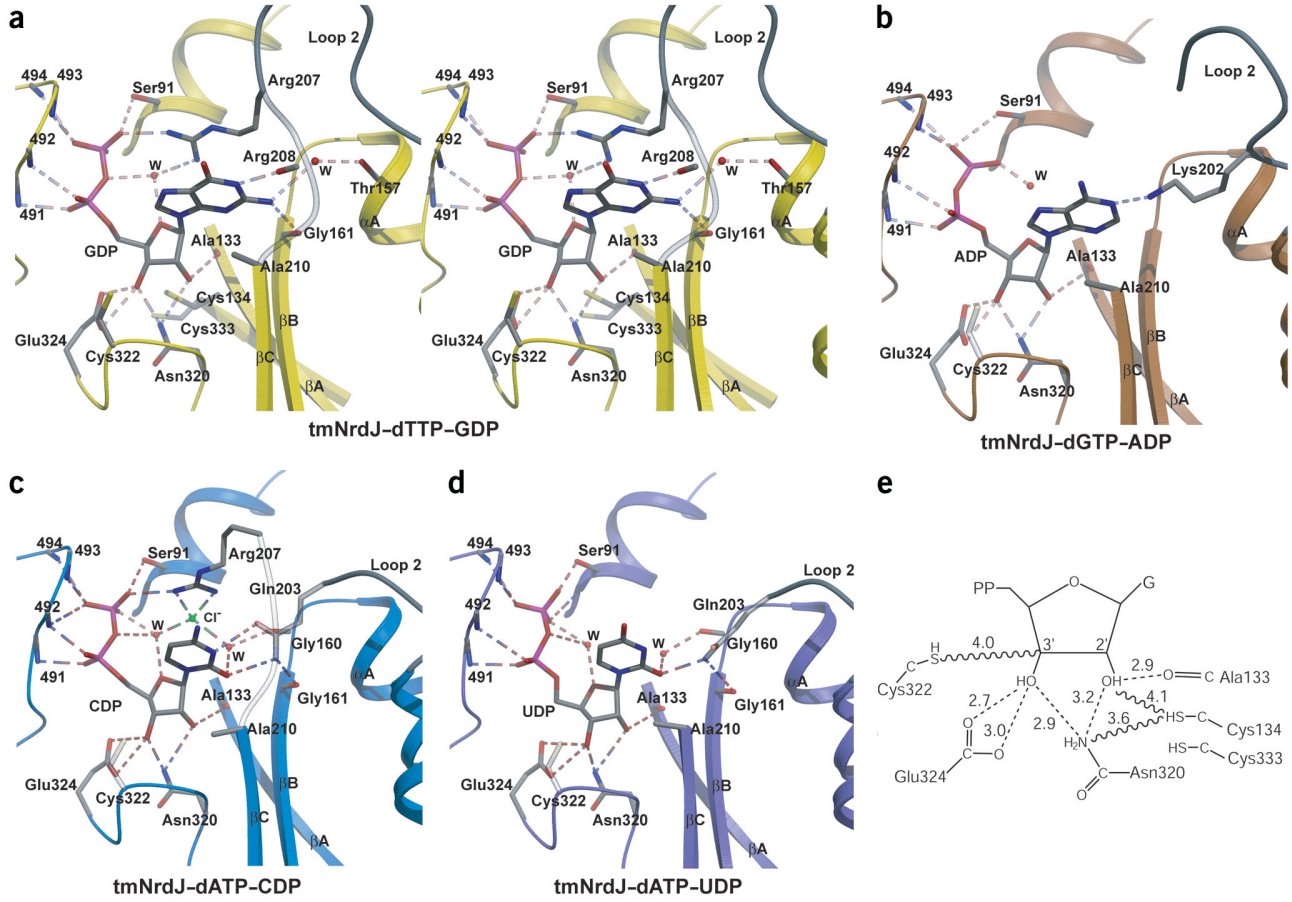

Figure 2 The active site structure of the different substrates in all four cognate substrate–effector complexes. (**a**–**d**) GDP (stereo view) (**a**) and mono views of ADP (**b**), CDP (**c**), and UDP (**d**). Loop 2 is highlighted in dark gray. (Water molecules not participating in direct base or ribose interactions have been omitted for clarity.) (**e**) Schematic diagram showing all interactions to the ribose of GDP (with distances).

The base position is essentially identical in the other substrate complexes. In particular, the glycosidic bond angle does not vary substantially. However, each substrate makes unique interactions to loop 2. In the dGTP–ADP structure (**Fig. 2b**), the main chain of loop 2 is disordered between residues 204 and 209. Residues 201–203 form an extra turn at the end of helix αB, resulting in the side chain of Lys202 being projected into the active site, making a hydrogen bond to the N1 atom of the substrate base. Finally, in the dATP–CDP (**Fig. 2c**) and dATP–UDP (**Fig. 2d**) complexes, loop 2 forms a truncated β-hairpin (ordered in the regions of residues 199–204 and 207–209 in dATP–CDP and in that of residues 199–203 in dATP–UDP), projecting Gln203 into the active site. In the dATP–CDP complex, Gln203 makes a bidentate hydrogen bond to the NH (N3) and CO (C2) groups of the substrate base whereas in the dATP–UDP complex it makes a single hydrogen bond to the substrate CO (C2). In the dATP–CDP complex, Arg207 clamps the substrate in a related but not identical way to the dTTP–GDP complex. In the dATP–UDP complex, Arg207 is not visible in the electron density.

Effector binding

The general deoxyribonucleotide-binding patterns are very similar for all three studied effectors, whether with or without their cognate substrates. As predicted by sequence comparision[14], the structure of the effector-binding site of the dimeric tmNrdJ class II RNR is highly similar to that in class I: the effectors fit into a pocket at the dimer interface with the α-phosphate anchored by the N terminus of αA′ of one monomer and the base projected toward loop 2 (residues 199–209) of the other monomer (see **Fig. 1b** for overall view and **Fig. 3a** for a detailed view). The β-hairpin loop 1 folds over the effector so that the nucleotide base is stacking in a hydrophobic pocket between loop 1 (residues 168–187) and the beginning of αA′ (at residue 143). The deoxyribose 3′ OH is bound by Asp141 and through a water molecule to the main chain amide group of Gly186 in loop 1. A putative magnesium ion is bound between the phosphate groups, coordinating three of the phosphate oxygen atoms. Further neutralization of the negative charge of the phosphates is made by Lys158 and Arg171.

Stabilization of loop 2

Loop 2 forms one distinctly different structure in every effector–substrate complex (**Fig. 3**), resulting in markedly different positioning of three key residues: Lys202, Gln203 and Arg207 (**Fig. 4**). In the purine-pyrimidine pair structures dTTP–GDP and dATP–CDP (**Fig. 3a**,**e**), loop 2 folds into the active site in β-hairpin-like conformations (partially disordered in the dATP–CDP structure). In the purine pair structure dGTP–ADP (**Fig. 3c**), loop 2 does not form a β-hairpin but instead an extra turn at the end of helix αB (residues 201–203), before becoming disordered. The side chain of Lys202 extends into the active site to hydrogen-bond to the substrate. A possible explanation

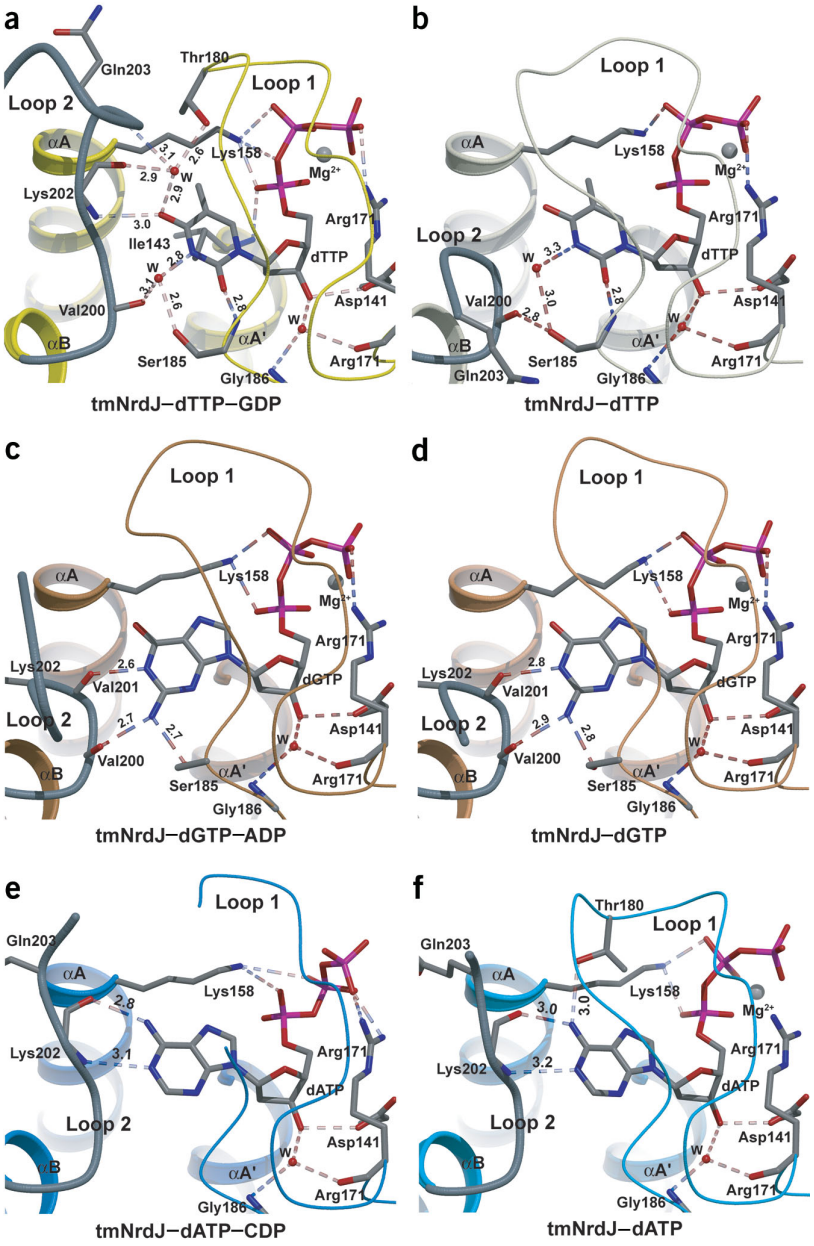

Figure 3 Effector interactions. Comparison of effector–substrate and effector-only complexes. (**a**) dTTP–GDP. (**b**) dTTP only. (**c**) dGTP–ADP. (**d**) dGTP only. (**e**) dATP–CDP. (**f**) dATP only. For the structure of dTTP–GDP, all interactions are shown except Phe190 stacking to the effector base, which is omitted for clarity. For the other effector complexes, some of the constant interactions around the deoxyribose and phosphates have also been omitted for clarity. The lengths of the hydrogen bonds to the effector base are indicated for all effector complexes. Loop 2 is highlighted in dark gray. The dATP–UDP structure has been omitted, as it is very similar to the dATP-only and dATP–CDP complexes in its base interactions. However its phosphate conformation is only similar to the dATP-only complex (including Mg^{2+}). In general, the phosphate-deoxyribose interactions are very similar in all structures, except in dATP–CDP, which apparently lacks a bound Mg^{2+} ion.

for the exclusion of the main chain atoms from the active site in the purine effector-substrate pair could be crowding in the loop 2 region due to the presence of the two large bases, whereas for the purine-pyrimidine pairs (dTTP–GDP and dATP–CDP) there is sufficient space to fit in the fully or partially ordered β-hairpins.

As most of the loop structures on the substrate-proximal side are disordered in the effector complexes determined without substrates, it seems that the final conformations seen in the substrate-bound forms are only partially stabilized by effector binding. In the effector-only structures with the purine effectors dGTP (**Fig. 3d**) and dATP (**Fig. 3f**), the same basic conformations of the effector-proximal region of loop 2 are seen as in the corresponding effector–substrate complexes (**Fig. 3c,e**, respectively). In the dGTP and dGTP–ADP complexes, the CO oxygen atoms of Val200 and Val201 make hydrogen bonds to NH (N2) and NH (N3) of dGTP, respectively, stabilizing the α-conformation of residues 201–203. In the dATP, dATP–CDP and dATP–UDP complexes, hydrogen bonds are instead made by the backbone carbonyl and amide groups of Lys202, to NH (N6) and N1, respectively, on the effector base, stabilizing the β-structures of loop 2 on the effector-proximal side (**Fig. 3e,f**).

In the structure of the dTTP–GDP complex, loop 2 displays a fully formed β-hairpin that makes four hydrogen bonds with the effector base (**Fig. 3a**), either directly, for example from the amide of Lys202 to CO (O4) on the base, or indirectly via water molecules, for example from the carbonyl of Gln203 and the amide nitrogen of Gly204 to CO (O4), and from the carbonyl of Val200 to N3. However, in contrast to the other effectors, the dTTP molecule in the effector-only structure is associated with a loop 2 conformation quite different from the β-hairpin observed in corresponding effector–substrate complex (**Fig. 3a**). The effector-proximal side of loop 2 folds instead into an α-helical structure (**Fig. 3b**). No hydrogen bonds are made by loop 2 to the effector and a positional shift of Ser185 creates a new hydrogen bond across the dimer interface. The effects of dTTP binding on loop 2 stabilization thus seem to differ from those of dATP and dGTP, where the key residues on loop 2 (Gln203 and Lys202, respectively) are apparently oriented toward the active site before substrate binding. This feature of dTTP could stem from differences in the initial binding of GDP to the active site compared to the binding of other substrates. The GDP base makes an important hydrogen bond interaction through its NH (N2) group directly to βB of the α/β barrel, rather than exclusively through loop 2 or coordinated waters as with the other substrates (**Fig. 2a**). GDP could therefore bind to the active site without having a preformed conformation of the active site portion of loop 2 and could thereafter stabilize its final conformation.

DISCUSSION

Ribonucleotide reductases have a complex system of allosteric regulation through feedback regulation by the triphosphate form of their products. The substrate conformations observed confirm the general substrate-binding mode found in the previous study of class I RNR[15];

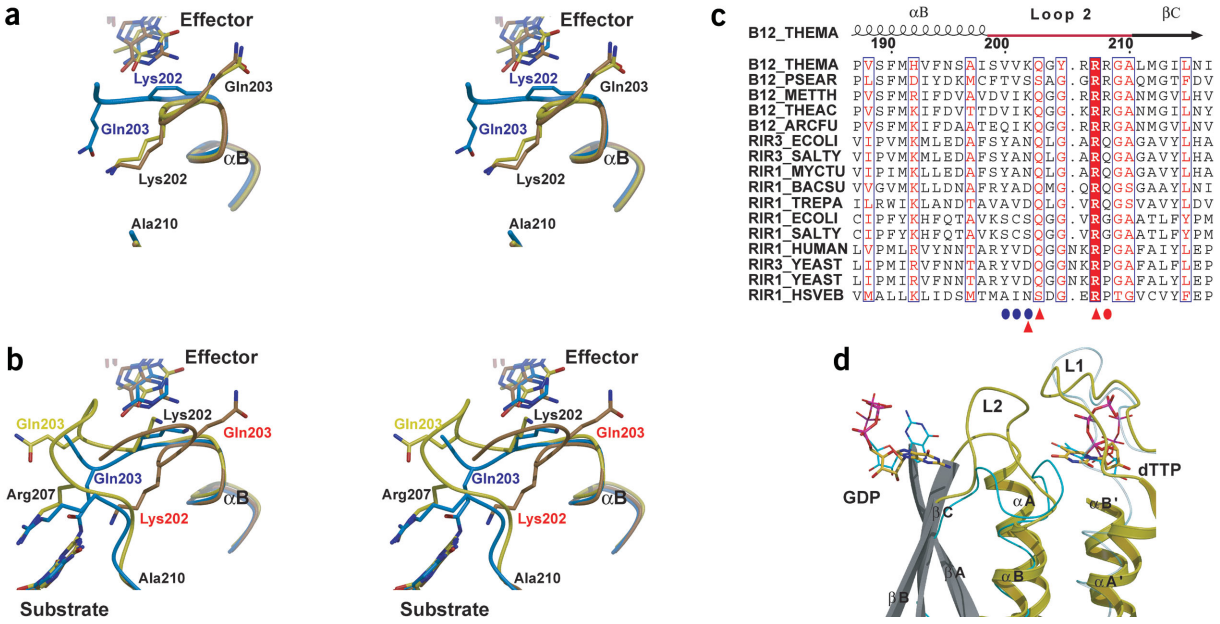

Figure 4 The structural flexibility of loop 2. (**a**) Superposition of loop 2 in the three effector-only structures (stereo view). Color labeling follows that in **Figures 2** and **3**: dTTP, yellow; dGTP, brown; dATP, blue. (**b**) Superposition of loop 2 with effector and substrate in three effector–substrate structures (stereo view). (The structure of dATP–UDP is very similar to dATP–CDP in this region and is not shown.) Color labeling corresponds to the structures with only effector: dTTP–GDP, yellow; dGTP–ADP, brown; dATP–CDP, blue. (**c**) Sequence alignment of loop 2 in classes I and II (a representative subset of available sequences). Residues of loop 2 involved in substrate and effector interactions are indicated at bottom of the alignment: side chain interactions, triangles; main chain interactions, dots (red, substrate interactions; blue, effector interactions). Class I sequences denoted with SWISS_PROT code and class II sequences are as follows: B12_THEMA, *T. maritima*; B12_PSEAE, *Pseudomonas aeruginosa*; B12_METTH, *Methanobacterium thermoautotrophicum*; B12_THEAC, *T. acidophilum*; B12_ARCFU, *Archaeoglobus fulgidus*. (**d**) A comparison of the effector-binding region of tmNrdJ (yellow) and *E. coli* R1 (cyan) in their respective dTTP–GDP complexes. The nucleotides belonging to the R1 dTTP–GDP structure and tmNrdJ are colored correspondingly. Note the difference in loop 2 conformations.

however, several important details of substrate conformation and interaction with the enzyme are revealed in the tmNrdJ structures owing to the high resolution and full occupancy. In particular, the ribose pucker is unambiguously established as C3′-*endo*. This may be essential to bring the H3′ atom close enough to Sγ of Cys322 in the active RNR to enable hydrogen atom abstraction[3,4]. Also, the orientation of the base is uniquely defined to direct the specific hydrogen bonding groups toward loop 2. Notably, several of the small amino acids at the end of loop 2 and at the beginning of βB, which are necessary to accommodate the GDP base when loop 2 is fully ordered, are among the very few conserved across all three classes of RNR[10], arguing for a similar substrate orientation in all RNRs.

The high-resolution complexes of RNR with cognate effector-substrate pairs allow for the first time a detailed analysis of the atomic basis for allosteric substrate specificity regulation in any RNR. Main chain atoms in residues 200–202 dominate the interactions with the specificity effector base. Different main chain arrangements proximal to the effector, in particular switching between stable α and β conformations, have marked effects on the conformation of loop 2, resulting in sufficient diversity to allow specific recognition of the different substrates (**Fig. 4a**). GDP is bound entirely by main chain atoms, whereas Lys202 is projected toward ADP and Gln203 toward CDP. These results confirm and reinforce the proposed role of loop 2 in transmission of the specificity signals[15]. Indeed it seems that loop 2 carries out the primary repertoire of conformational changes and that the differences seen in other loops (such as loop 1), both here and in R1, are compensatory, in that the monomer containing αA′ and loop 1 simply acts as an anchor for the effector, whereas loop 2 of the other monomer is active in signaling. No further major role for subunit-subunit interactions in the regulatory events is obvious from the present data.

Cooperativity in loop 2 stabilization

The structural flexibility of loop 2 is clearly at the heart of the mechanism for specificity regulation, as the enzyme seems to be set up for a dynamic equilibrium between different loop 2 conformations. The binding of the different effectors shifts this equilibrium toward a state favoring initial capture of the corresponding cognate substrate, with a subsequent ordering of loop 2 that involves the substrate to various degrees. In two of the effector-only complexes, dATP and dGTP, the final loop 2 structure is already substantially preformed (compare **Fig. 4a**,**b**). In contrast, the complex with dTTP alone does not show the ordered active site part of loop 2, which is observed in the structure of the cognate pair dTTP–GDP (**Fig. 4a**,**b**). This difference suggests a higher degree of cooperativity between substrate binding and the formation of the final active site structure (that is, loop 2) for the effector dTTP. This apparent substrate cooperativity in the ordering of loop 2 fits well with previous results suggesting two-way communication between the active site and the specificity site. In ultrafiltration binding studies of mouse R1 protein[23], GDP was observed to enhance the binding of its cognate effector dTTP, whereas CDP strongly inhibited binding of the non-cognate effector dGTP. This did not depend on competition of NDPs for the effector site, as the effects were reduced by competition between GDP and ADP for the active site. Furthermore, earlier studies of radiolabeled effector incorporation into *E. coli* R1 also showed cooperativity between substrate and effector binding[24] and, notably, the influence of GDP on dTTP

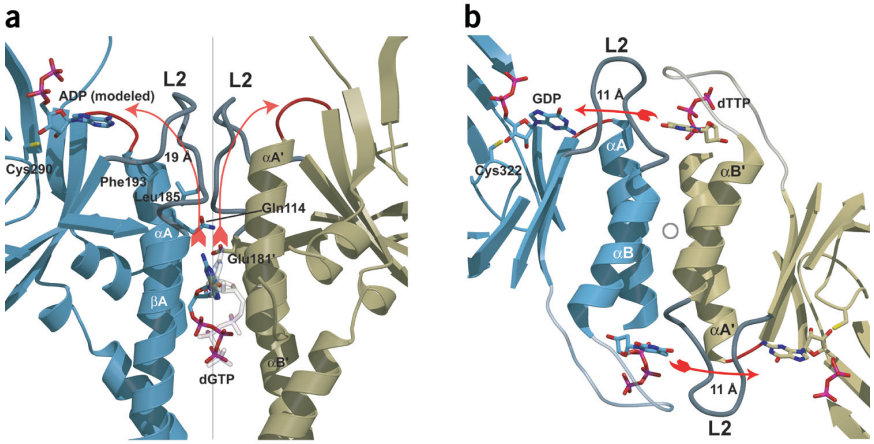

Figure 5 Comparison of the regions involved in allosteric specificity regulation in class III and class I-II RNRs. The two families are represented by structures of nucleotide complexes showing a well-defined loop 2. (**a**) Bacteriophage T4 NrdD (class III) containing dGTP and ADP modeled using its position in the present work (ATP is the true substrate). (**b**) tmNrdJ with dTTP and GDP. The shortest paths between effector and substrate are shown in red for the two-fold related pathways in both classes. Loop 2 (L2) is transparent dark gray. The dimer axes are shown in both panels, as a vertical line in **a** and as a circle in **b**. The allosteric signal in the class I-II family is transmitted through loop 2 over a distance of 11 Å, whereas in the class III structure it is transmitted over a larger distance (19 Å) through a chain of residues making van der Waals contacts (Gln114, Leu185 and Pro193), of which all but Gln114 are in loop 2.

incorporation was strongest. The structural data strongly support the hypothesis that the active site can 'talk back' to the specificity site.

Although the present study maps conformational changes leading to the final substrate binding through complementary hydrogen bond interactions made from loop 2 and βB, it is hard to judge the relative contributions of effector and substrate to the energetics of the events. Furthermore, the specificity regulation is not absolute, but rather stimulatory, as a basal level of turnover of noncognate substrate is observed. Further insights could thus be obtained from structural studies of noncognate complexes.

The nucleotide-binding experiments presented here were carried out at room temperature, whereas the enzyme has its optimal activity at 90 °C. It has been found that CDP reduction by tmNrdJ is not stimulated by dATP at temperatures < 60 °C (ref. 9). However, from our structural studies it is clear that loop 2 has sufficient flexibility at room temperature to undergo major conformational transitions. Furthermore, the adaptation of the hydrogen bonding pattern of the groups presented by the protein to the unique pattern on the base, also involving conserved residues for key interactions, is highly unlikely to be artifactual. Therefore the loss of activity at lower temperatures is probably due to other factors, such as conformational changes upon coenzyme B12 binding, as seen in llNrdJ, or less effective use of the radical chemistry.

Evolutionary implications

Owing to the strong sequence similarity between class I and II RNRs in loop 2 (sequence alignment in **Fig. 4c**) and the structural conservation of the dimer interface (structural comparison in **Fig. 4d**), it seems likely that the results are of general significance for both classes of RNR. In particular, the key residues in loop 2, Gln203, Arg207 and Ala210, are completely or almost completely conserved. Somewhat surprisingly, Lys202 is not conserved (**Fig. 4c**), although it makes an important hydrogen bond to N3 of ADP. This residue can also be aspartate, asparagine or serine in other class I and II sequences, and although all of these are polar residues, the detailed hydrogen bonding interactions with ADP in the other RNRs must be achieved differently.

The use of Arg207 as a substrate clamp in the dTTP–GDP and dATP–CDP complexes (**Fig. 2a,d**) constitutes a notable mode of locking the substrate into the active site. However, even though Arg207 is completely conserved, it apparently does not participate in binding of ADP or UDP. In the case of ADP, the most likely explanation is that as Lys202 stretches over to interact with the substrate base (**Fig. 3c** and **4b**), the Arg207 main chain position required for the side chain to clamp is sterically excluded by the Lys202 side chain. In the dATP–UDP complex there is no electron density indicating the presence of an arginine clamp (**Fig. 2e**), but here the reasons may be subtler, as a slight reorientation of the substrate-proximal part of loop 2 seems to occur owing to the reorientation of Gln203 relative to the dATP–CDP complex (**Fig. 2d**).

The common evolutionary origin of the three classes of RNRs is firmly established through the conservation of the α/β barrel and the core of the catalytic machinery[17–19]. Although the regulatory effect of effector binding on deoxyribonucleotide production is very similar in the three enzyme classes, the large differences in dimer formation in class III RNRs[17] (**Fig. 5**), as well as in the position of the specificity site in relationship to the active site[10,17], do at first glance argue strongly for a completely different mechanism of regulation in the class III system as compared with the class I-II system. However, there are notable similarities in the structural effects of effector binding between the two systems (**Fig. 5**). In both, the stabilization of different loop 2 conformers by effector binding is a key regulatory component in that specificity regulation in both systems involves transitions between α and β conformations of the effector-proximal region of loop 2. Furthermore, glycine residues in turn B and the following strand βB, which in tmNrdJ are involved in base recognition of GDP, are also conserved in class III RNRs, indicating the conservation of the position of the substrate base in relationship to loop 2. The structures therefore support a divergent evolutionary scenario where interactions have switched while conserving essential elements such as signaling through loop 2 (**Fig. 5**). In class III the signal is transmitted over a greater distance than in class I and II, but still results in a refolding of the substrate-proximal side of loop 2.

In summary, substrate specificity signaling is achieved structurally through the effectors shifting what seems to be a dynamic equilibrium between different loop 2 conformations, providing the essential elements for cognate substrate recognition. On the basis of sequence conservation, the key conformational events are conserved in all RNRs, especially the α-to-β remodeling of loop 2, which seems to be a unique and unifying aspect in specificity regulation for all RNR classes.

METHODS

Crystallization and nucleotide soaking experiments. A C-terminally truncated construct of the *T. maritima* class II ribonucleotide reductase, tmNrdJ, corresponding to the TM2 70-kDa proteolytic fragment (residues 1–644), was subcloned from the pET22b-derived plasmid pUA724 (ref. 14). A 0.35-kilobase

Table 1 Data statistics

	dATP	dTTP	dGTP	dTTP–GDP	dGTP–ADP[b]	dATP–CDP	dATP–UDP[b]
Effector (mM)	Cocrystal	0.4	0.8	0.4	0.8	0.8	0.8
Substrate (mM)	–	–	–	2	16	8	8
$MgCl_2$ (mM)	–	3.3	13.2	3.3	13.2	6.6	6.6
Data collection							
Beamlines	I711	X13	I711	X11	I711	X11	X13
Resolution (Å)[a]	25–2.40 (2.6–2.4)	20–2.40 (2.6–2.4)	42.0–1.86 (2.0–1.86)	18–1.90 (1.97–1.90)	25–2.15 (2.30–2.15)	20–2.25 (2.50–2.25)	25–2.50 (2.56–2.50)
Unit cell dimensions							
a, b, c (Å)	116, 124, 107	118, 124, 106	188, 124, 106	119, 124, 107	118, 123, 106	106, 124, 117	118, 123, 106
β (°)	104	104	104	104	103	104	103
Completeness (%)[a]	99.3 (99.5)	99.6 (99.5)	99.8 (100.0)	97.2 (96.6)	97.2 (96.9)	99.3 (99.7)	99.9 (100)
Observed reflections	214,821	219,194	650,037	313,127	168,419	411,446	210,356
Unique reflections	57,137	57,953	124,131	115,971	77,677	138,333	51,412
$\langle I / \sigma \rangle$[a]	12.1 (3.24)	8.4 (3.93)	12.23 (3.43)	12.7 (3.20)	8.91 (2.48)	7.99 (3.20)	21.5 (3.77)
R_{merge}[a]	6.3 (38.8)	11.5 (33.7)	6.6 (40.0)	7.0 (39.9)	4.9 (28.9)	9.7 (36.8)	6.0 (38.0)
Refinement							
R_{cryst}	21.1	20.9	20.9	18.2	20.9	19.1	21.5
R_{free}	25.2	25.9	24.1	22.1	24.7	25.1	26.7
Nonhydrogen atoms	9,994	9,802	10,034	10,853	10,025	20,320	10,068
Water molecules	261	112	334	791	256	644	199
R.m.s. deviations							
Bond lengths (Å)	0.019	0.020	0.021	0.019	0.019	0.020	0.020
Bond angles (°)	1.69	1.69	1.70	1.75	1.65	1.78	1.82
Average *B*-factor (Å^2)	44.6	39.6	29.6	31.6	48.0	31.8	43.6

All crystals were in space group *C*2 with one dimer in the asymmetric unit, except for dATP–CDP, which was in space group $P2_1$ with two dimers in the asymmetric unit. These crystals exhibit strong pseudo-*C*2 symmetry.

[a]Values in parentheses are for the highest-resolution shell. [b]Data reduction was done using DENZO/SCALEPACK[26].

(kb) fragment amplified from pUA724 by PCR, using Taq polymerase with primers PrD (5′-TACGTGAACCAGGT-3′ and PrALKT (5′-CCAGGATCCTAT-GTTTTCAAGGCTT -3′), was digested with HindIII-BamHI to generate a 0.27-kb fragment that substituted for a 1-kb HindIII-BamHI fragment in pUA724. The resulting plasmid, pIG12, was used for overexpression in *E. coli* BL21(DE3) and the protein was purified as described[8], with the addition of an overnight dialysis step in 20 mM Tris-Cl, pH 7.6, and 5 mM DTT.

TmNrdJ crystals were obtained in hanging drops at 14–20 °C with a precipitant solution consisting of 8–12% (w/v) PEG 8000 (Sigma), 0.1 M sodium acetate, pH 4.5, 0.1 M NaCl, 5–15% (v/v) glycerol and 10 mM DTT. The best crystals appeared after 3–5 d in 4 + 2 µl (protein + precipitant) drops using an 11 mg ml^{-1} protein solution. Crystal mother liquor containing 20% (v/v) glycerol was used as cryoprotectant (cryo) solution.

In the nucleotide soaking experiments, single crystals were incubated for 3–4 h at 20–25 °C in 3 µl drops on coverslips over 300 µl of cryo solution. The soaking solutions consisted of a 1.6× concentrated cryo solution, to which nucleotide(s), $MgCl_2$, DTT and water were added to obtain a 1× solution. Final magnesium and nucleotide concentrations are listed in **Table 1**.

Data collection and processing. All crystals were frozen in liquid nitrogen after a minimum of 1–2 min in cryo solution and data collection was carried out at 100 K. European Molecular Biology Laboratory beamlines X11 and X13 at Deutsches Elektronen-Synchrotron, beamline ID29 at the European Synchrotron Radiation Facility, and beamline I711 at MAX-lab were used as X-ray sources. The data were processed and scaled with XDS or HKL[25,26]. The crystals belong to either space group *C*2 or $P2_1$ with a pseudo-*C*2 symmetry. Data statistics are listed in Table 1. The CCP4 suite was used for all subsequent crystallographic data manipulations[27,28].

Structure determination and refinement. The structure of the 'native' dimeric tmNrdJ (later found to contain residual dATP from the purification procedure) was solved with molecular replacement using an *E. coli* R1 dimer structure (PDB entry 1RLR), trimmed of loops and mutated into a polyserine model while conserved residues (15% of sequence) were retained. Molecular replacement and refinement were done using CNS[29]. The correct solution in space group *C*2 consisted of one dimer per asymmetric unit. After initial model building, phases were improved with RESOLVE[30], using two-fold non-crystallographic symmetry (NCS) and prime and switch phasing. Structure factors were obtained from a dGTP–ADP soaked crystal with data to a resolution of 2.35 Å (not shown) and the initial phases from a partial model with an R_{free} and R of 43.0 and 41.0, respectively. The resulting maps allowed rapid manual model building.

Initial nucleotide coordinates were obtained from the HICUP server[31]. REFMAC5 (ref. 32) topology or CNS[29] parameter and topology files were generated using the PRODRG server[33]. The different nucleotide-protein or protein structures were isomorphous and new structures were determined using high-resolution tmNrdJ structures as starting models in refinement, without recourse to molecular replacement. Except for the refinement of the 1.9-Å dTTP–GDP structure, two-fold or four-fold NCS restraints were applied in all initial refinements either in CNS[29] or REFMAC5 (ref. 32). All manual model building was done in QUANTA (Accelrys). For some structures ARP/wARP[34] was used for phase improvement and water addition. All figures were made using MolScript[35], BobScript[36] and Raster3D[37].

Coordinates. The structures have been deposited in the Protein Data Bank (accession codes: 1XJF, dATP complex (native); 1XJG, dATP–UDP complex; 1XJN, dATP–CDP complex; 1XJM, dTTP complex; 1XJE, dTTP–GDP complex; 1XJJ, dGTP complex; 1XJK, dGTP–ADP complex).

ACKNOWLEDGMENTS

We thank staff at beamline I711 of MAX-lab (Y. Cerenius) and at the European Molecular Biology Laboratory Hamburg outstation (C. Enroth) for technical

help with data collection. This work was supported by grants from the Swedish Research Council (to D.L. and P.N.) and Karolinska Institutet (to P.R.).

COMPETING INTERESTS STATEMENT

The authors declare that they have no competing financial interests.

Received 19 March; accepted 13 August 2004
Published online at http://www.nature.com/nsmb/

1. Jordan, A. & Reichard, P. Ribonucleotide reductases. *Annu. Rev. Biochem.* **67**, 71–98 (1998).
2. Fontecave, M., Mulliez, E. & Logan, D.T. Deoxyribonucleotide synthesis in anaerobic microorganisms: the class III ribonucleotide reductase. *Prog. Nucleic Acid Res. Mol. Biol.* **72**, 95–127 (2002).
3. Stubbe, J., Ator, M. & Krenitsky, T. Mechanism of ribonucleoside diphosphate reductase from *Escherichia coli*. Evidence for 3′-C–H bond cleavage. *J. Biol. Chem.* **258**, 1625–1631 (1983).
4. Stubbe, J. Ribonucleotide reductases. *Adv. Enzymol. Relat. Areas Mol. Biol.* **63**, 349–419 (1990).
5. Reichard, P. Ribonucleotide reductases: the evolution of allosteric regulation. *Arch. Biochem. Biophys.* **397**, 149–155 (2002).
6. Kunz, B.A. *et al.* International Commission for Protection Against Environmental Mutagens and Carcinogens. Deoxyribonucleoside triphosphate levels: a critical factor in the maintenance of genetic stability. *Mutat. Res.* **318**, 1–64 (1994).
7. Brown, N.C. & Reichard, P. Role of effector binding in allosteric control of ribonucleoside diphosphate reductase. *J. Mol. Biol.* **46**, 39–55 (1969).
8. Eliasson, R., Pontis, E., Jordan, A. & Reichard, P. Allosteric control of three B_{12}-dependent (class II) ribonucleotide reductases. Implications for the evolution of ribonucleotide reduction. *J. Biol. Chem.* **274**, 7182–7189 (1999).
9. Andersson, J., Westman, M., Hofer, A. & Sjoberg, B.-M. Allosteric regulation of the class III anaerobic ribonucleotide reductase from bacteriophage T4. *J. Biol. Chem.* **275**, 19443–19448 (2000).
10. Larsson, K.M., Andersson, J., Sjoberg, B.M., Nordlund, P. & Logan, D.T. Structural basis for allosteric substrate specificity regulation in anaerobic ribonucleotide reductases. *Structure* **9**, 739–750 (2001).
11. Beck, W.S. Regulation of cobamide-dependent ribonucleotide reductase by allosteric effectors and divalent cations. *J. Biol. Chem.* **242**, 3148–3158 (1967).
12. Panagou, D., Orr, M.D., Dunstone, J.R. & Blakley, R.L. A monomeric, allosteric enzyme with a single polypeptide chain. Ribonucleotide reductase from *Lactobacillus leichmannii*. *Biochemistry* **11**, 2378–2388 (1972).
13. Chen, A.K., Bhan, A., Hopper, S., Abrams, R. & Franzen, J.S. Substrate and effector binding to ribonucleoside triphosphate reductase of *Lactobacillus leichmannii*. *Biochemistry* **13**, 654–661 (1974).
14. Jordan, A. *et al.* B12-dependent ribonucleotide reductases from deeply rooted eubacteria are structurally related to the aerobic enzyme from *Escherichia coli*. *Proc. Natl. Acad. Sci. USA* **94**, 13487–13492 (1997).
15. Eriksson, M. *et al.* Binding of allosteric effectors to ribonucleotide reductase protein R1: reduction of active-site cysteines promotes substrate binding. *Structure* **5**, 1077–1092 (1997).
16. Uppsten, M. *et al.* Structure of the large subunit of class Ib ribonucleotide reductase from *Salmonella typhimurium* and its complexes with allosteric effectors. *J. Mol. Biol.* **330**, 87–97 (2003).
17. Logan, D.T., Andersson, J., Sjöberg, B.M. & Nordlund, P. A glycyl radical site in the crystal structure of a class III ribonucleotide reductase. *Science* **283**, 1499–1504 (1999).
18. Sintchak, M.D., Arjara, G., Kellogg, B.A., Stubbe, J. & Drennan, C.L. The crystal structure of class II ribonucleotide reductase reveals how an allosterically regulated monomer mimics a dimer. *Nat. Struct. Biol.* **9**, 293–300 (2002).
19. Uhlin, U. & Eklund, H. Structure of ribonucleotide reductase protein R1. *Nature* **370**, 533–539 (1994).
20. Becker, A. *et al.* Structure and mechanism of the glycyl radical enzyme pyruvate formate-lyase. *Nat. Struct. Biol.* **6**, 969–975 (1999).
21. Eklund, H. & Fontecave, M. Glycyl radical enzymes: a conservative structural basis for radicals. *Structure Fold Des.* **7**, R257–R262 (1999).
22. Himo, F. & Siegbahn, P.E. Quantum chemical studies of radical-containing enzymes. *Chem. Rev.* **103**, 2421–2456 (2003).
23. Chimploy, K. & Mathews, C.K. Mouse ribonucleotide reductase control: influence of substrate binding upon interactions with allosteric effectors. *J. Biol. Chem.* **276**, 7093–7100 (2001).
24. Eriksson, S. Direct photoaffinity labeling of ribonucleotide reductase from Escherichia coli. Evidence for enhanced binding of the allosteric effector dTTP by the presence of substrates. *J. Biol. Chem.* **258**, 5674–5678 (1983).
25. Kabsch, W. Automatic processing of rotation diffraction data from crystals of initially unknown symmetry and cell constants. *J. Appl. Cryst.* **26**, 795–800 (1993).
26. Otwinowski, Z. & Minor, W. Processing of X-ray diffraction data collected in oscillation mode. *Methods Enzymol.* **276**, 307–326 (1997).
27. Collaborative Computational Project, Number 4. The CCP4 suite: programs for protein crystallography. *Acta Crystallogr. D* **50**, 760–763 (1994).
28. Potterton, E., Briggs, P., Turkenburg, M. & Dodson, E. A graphical user interface to the CCP4 program suite. *Acta Crystallogr. D* **59**, 1131–1137 (2003).
29. Brünger, A.T. *et al.* Crystallography & NMR system: a new software suite for macromolecular structure determination. *Acta Crystallogr. D* **54**, 905–921 (1998).
30. Terwilliger, T.C. Maximum-likelihood density modification. *Acta Crystallogr. D* **56**, 965–972 (2000).
31. Kleywegt, G.J. & Jones, A. Databases in protein crystallography. *Acta Crystallogr. D* **54**, 1119–1131 (1998).
32. Murshudov, G.N., Vagin, A.A. & Dodson, E.E. Refinement of macromolecular structures by the maximum-likelihood method. *Acta Crystallogr. D* **54**, 240–255 (1997).
33. van Aalten, D.M. *et al.* PRODRG, a program for generating molecular topologies and unique molecular descriptors from coordinates of small molecules. *J. Comput. Aided Mol. Des.* **10**, 255–262 (1996).
34. Perrakis, A., Sixma, T.K., Wilson K.S. & Lamzin, V.S. wARP: improvement and extension of crystallographic phases by weighted averaging of multiple refined dummy atomic models. *Acta Crystallogr. D* **53**, 448–455 (1997)
35. Kraulis, P.J. MOLSCRIPT: a program to produce both detailed and schematic plots of protein structures. *J. Appl. Crystallogr.* **24**, 946–950 (1991).
36. Esnouf, R.M. An extensively modified version of MolScript that includes greatly enhanced coloring capabilities. *J. Mol. Graph. Model.* **15**, 132–4, 112–113 (1997).
37. Merritt, E.A. & Murphy, M.E.P. Raster3D version 2.0: a program for photorealistic molecular graphics. *Acta Crystallogr. D* **50**, 869–873 (1994).